2020 IEEE International Conference on Robotics and Automation (ICRA)
31 May - 31 August, 2020. Paris, France

Optimal Fast Entrainment Waveform for Indirectly Controlled Limit Cycle Walker Against External Disturbances

Longchuan Li[1], Isao Tokuda[2] and Fumihiko Asano[3]

***Abstract*— After occasional perturbation, it is crucial to spontaneously control the limit cycle walking so that it quickly returns to its closed orbit in phase space. Otherwise, its stability can not be sufficiently guaranteed if the speed of recovery is slow while successive perturbation is applied. The accumulated deviation may eventually drive the phase outside the basin of attraction, leading to failure of the walking. In this sense, a control law that quickly recovers the disturbed phase before encountering the following perturbations is indispensable. With this consideration, here we analytically derive an optimal fast entrainment waveform that maximizes the speed of phase recovery based on phase reduction theory. Our theoretical method is numerically evaluated using a limit cycle walker, which is indirectly controlled by the oscillation of a wobbling mass via entrainment effect. The obtained waveform is used as the desired trajectory of the wobbling motion. The simulation results show that the waveform we derived achieves the best performance among all candidates. Our method helps to enhance the stability of limit cycle walking.**

I. INTRODUCTION

Limit cycle walking [1], inspired by passive dynamic walking [2], is one of the most prospective methods in terms of speed and efficiency. To implement such gait in real tasks, plenty of researchers focused on the issue of strengthening the robustness of limit cycle walking against external disturbances and achieved superb results [3]–[5]. In contrast to the success they achieved, comparatively little work has been done on reducing the number of steps required for returning to the limit cycle after being disturbed. This issue, however, deserves great concern, since a longer transient potentially leads to accumulated deviation, give rise to a failed locomotion. To fill this gap, Asano and Xiao proposed a deceleration-based method which increases the convergence speed to limit cycle by either actively implementing a braking effect or passively utilizing the viscosity effect after overcoming the potential barrier [6]. As a trade-off, the steady walking speed is also decreased, unfortunately.

To make the walking quickly converge to the limit cycle without impairing its performance, positively utilizing the natural dynamics of the system is necessary. Therefore we adopt a novel walking paradigm, namely indirectly controlled limit cycle walking [7]. As illustrated in Fig. 1, the walking machine is composed of two identical eight-legged rimless wheels, which are assumed to be synchronized ($\theta_1 \equiv \theta_2$) and are connected by a beam. The beam is, therefore, always parallel to the ground, benefit from such configuration. In parallel with the beam, an active wobbling mass that oscillates periodically is attached to it to indirectly control the frequency of the walking. The oscillation of the wobbling mass not only has a potential to enhance energy efficiency by suspending a load [8] [9], but also entrains the frequency and phase of the limit cycle locomotion, which is similar to the vibration of viscera in biological systems [10] [11].

As the authors observed previously [12] [13], the dynamics of these underactuated robots are highly nonlinear. Therefore we approximate the system as a phase oscillator based on the phase reduction theory [14]. Accordingly, we derive an optimal fast entrainment waveform as a desired oscillation trajectory for the wobbling mass, where the convergence speed of phase is maximized with power constraint. Our method is model-free and independent of the state of the walker. Although the trajectory tracking of the wobbling mass needs the feedback of itself, it can be easily measured and controlled by an encoder in real-time. To make an evaluation, we numerically compare our waveform with two standard examples. Simulation results suggest that the waveform we derived requires the least steps for returning to the entrained limit cycle after perturbation among all candidates. Our theoretical method contributes to increasing the convergence speed of limit cycle walking, which potentially enhances the robustness of the walker in the real tasks with the existence of successive perturbations.

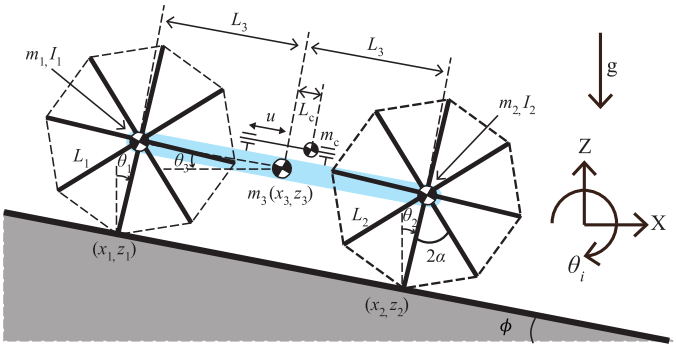

Fig. 1: Combined rimless wheels with active wobbling mass

*This work was partially supported by Grants-in-Aid for Science Research, 19K04255 and 17H06313, provided by the Japan Society for the Promotion of Science (JSPS)

[1]Longchuan Li is with the Research Organization of Science and Technology, Ritsumeikan University, 1-1-1 Nojihigashi, Kusatsu, Shiga 525-8577, Japan llt t2144@fc.ritsumei.ac.jp

[2]Isao Tokuda is with the Department of Mechanical Engineering, Ritsumeikan University, 1-1-1 Nojihigashi, Kusatsu, Shiga 525-8577, Japan isao@fc.ritsumei.ac.jp

[3]Fumihiko Asano is with the School of Information Science, Japan Advanced Institute of Science and Technology, 1-1 Asahidai, Nomi, Ishikawa 923-1292, Japan fasano@jaist.ac.jp

II. DYNAMICS AND CONTROL

In this section, we briefly introduce the system dynamics of this walker and indirectly controlling mechanism, as preparations for implementing our method. One can refer to [7] and [15] for detailed explanation.

A. Equation of Motion

Let $\boldsymbol{q}$ be the generalized coordinate vector. The equation of motion and holonomic constraints of this system then becomes:

$$\boldsymbol{M}(\boldsymbol{q})\ddot{\boldsymbol{q}}+\boldsymbol{h}(\boldsymbol{q},\dot{\boldsymbol{q}}) = \boldsymbol{J}(\boldsymbol{q},\dot{\boldsymbol{q}})^{\mathrm{T}}\boldsymbol{\lambda}+\boldsymbol{S}u, \quad (1)$$

$$\boldsymbol{J}(\boldsymbol{q},\dot{\boldsymbol{q}})\dot{\boldsymbol{q}} = \boldsymbol{0}_{n\times 1}. \quad (2)$$

In Eq. (1), $\boldsymbol{M}(\boldsymbol{q})$ represents the inertia matrix, $\boldsymbol{h}(\boldsymbol{q})$ represents the combination of centrifugal force, Coriolis force and gravity terms. Besides, $\boldsymbol{J}(\boldsymbol{q},\dot{\boldsymbol{q}})$ is the Jacobian matrix for holonomic constraints and $\boldsymbol{\lambda}$ is the constraint forces vector. $\boldsymbol{S}$ is the driving vector and u is the control input. In Eq. (2), n is the quantity of holonomic constraints. According to Eq. (1), the dynamics of $\boldsymbol{q}$ can be solved as:

$$\ddot{\boldsymbol{q}} = \boldsymbol{M}^{-1}(\boldsymbol{J}^{\mathrm{T}}\boldsymbol{\lambda}+\boldsymbol{S}u-\boldsymbol{h}), \quad (3)$$

where the constraint forces vector $\boldsymbol{\lambda}$ is derived by taking time derivative on both sides of Eq. (2) and solving the resultant equation with Eq. (1) simultaneously:

$$\boldsymbol{\lambda} = (\boldsymbol{J}\boldsymbol{M}^{-1}\boldsymbol{J}^{\mathrm{T}})^{-1}(\boldsymbol{J}\boldsymbol{M}^{-1}(\boldsymbol{h}-\boldsymbol{S}u)-\dot{\boldsymbol{J}}\dot{\boldsymbol{q}}). \quad (4)$$

B. Collision Equation

We assume that the rear feet of the walker leave the ground immediately after the landing of the fore feet according to the inelastic collision model. The update of the velocity of coordinate matrix becomes:

$$\boldsymbol{M}(\boldsymbol{q})\dot{\boldsymbol{q}}^{+} = \boldsymbol{M}(\boldsymbol{q})\dot{\boldsymbol{q}}^{-}+\boldsymbol{J}_I(\boldsymbol{q})^{\mathrm{T}}\boldsymbol{\lambda}_I, \quad (5)$$

$$\boldsymbol{J}_I(\boldsymbol{q})\dot{\boldsymbol{q}}^{+} = \boldsymbol{0}_{n\times 1}, \quad (6)$$

where the superscripts $+$ and $-$ represent the instant immediately after and before landing, and $\boldsymbol{J}_I(\boldsymbol{q})$ and $\boldsymbol{\lambda}_I$ represent the constraints matrix and constraint forces vector at landing instant. By multiplying $\boldsymbol{M}^{-1}$ on both sides of Eq. (5), the velocity vector becomes:

$$\dot{\boldsymbol{q}}^{+} = \dot{\boldsymbol{q}}^{-}+\boldsymbol{M}^{-1}\boldsymbol{J}_I^{\mathrm{T}}\boldsymbol{\lambda}_I, \quad (7)$$

where the constraint forces vector in the collision equation can be derived by solving Eq. (6) and (7) simultaneously:

$$\boldsymbol{\lambda}_I = -(\boldsymbol{J}_I\boldsymbol{M}^{-1}\boldsymbol{J}_I^{\mathrm{T}})^{-1}\boldsymbol{J}_I\dot{\boldsymbol{q}}^{-}. \quad (8)$$

C. Indirectly Controlling Mechanism

Under the framework of indirectly controlling mechanism, no torque is applied at any joint, instead, the walker's dynamics is indirectly controlled by the periodically oscillation of the wobbling mass. The driving vector $\boldsymbol{S}$, therefore, specifies the actuation on the wobbling mass, and the control input u enables the trajectory of wobbling mass to follow a desired waveform. Accordingly, the displacement of the wobbling mass L_c becomes the control output, *i.e.*, $L_c = \boldsymbol{S}^{\mathrm{T}}\boldsymbol{q}$. By taking its second-order derivative with respect to time, the relationship between input and output is linearized as:

$$\begin{aligned}\ddot{L_c} &= \boldsymbol{S}^{\mathrm{T}}\ddot{\boldsymbol{q}}\\ &= \boldsymbol{S}^{\mathrm{T}}\boldsymbol{M}^{-1}\left(\boldsymbol{Y}(\boldsymbol{S}u-\boldsymbol{h})-\boldsymbol{J}^{\mathrm{T}}\boldsymbol{X}^{-1}\dot{\boldsymbol{J}}\dot{\boldsymbol{q}}\right) = Au-B, \quad (9)\end{aligned}$$

where

$$\boldsymbol{X} := \boldsymbol{J}\boldsymbol{M}^{-1}\boldsymbol{J}^{\mathrm{T}}, \quad \boldsymbol{Y} := \boldsymbol{I}-\boldsymbol{J}^{\mathrm{T}}\boldsymbol{X}^{-1}\boldsymbol{J}\boldsymbol{M}^{-1},$$
$$A := \boldsymbol{S}^{\mathrm{T}}\boldsymbol{M}^{-1}\boldsymbol{Y}\boldsymbol{S}, \quad B := \boldsymbol{S}^{\mathrm{T}}\boldsymbol{M}^{-1}(\boldsymbol{Y}\boldsymbol{h}+\boldsymbol{J}^{\mathrm{T}}\boldsymbol{X}^{-1}\dot{\boldsymbol{J}}\dot{\boldsymbol{q}}),$$

and $\boldsymbol{I}$ is an identity matrix that has the same size as $\boldsymbol{M}$. The control input u that enables the wobbling trajectory $L_c(t)$ to track a desired waveform $F(t)$ is defined as

$$u = A^{-1}(v+B), \quad (10)$$

$$v = \ddot{F}(t)+K_{\mathrm{D}}(\dot{F}(t)-\dot{L}_c(t))+K_{\mathrm{P}}(F(t)-L_c(t)), \quad (11)$$

where K_{D} [s^{-1}] and K_{P} [s^{-2}] are the PD control gains.

III. METHOD

In this section, we introduce our method of deriving an optimal fast entrainment waveform as the desired trajectory $F(t)$ for the wobbling mass.

A. Phase Entrainment

By excluding the ground landing event, the continuous dynamics of the indirectly controlled limit cycle walking can be approximated by following phase equation [18] [19] according to phase reduction theory:

$$\dot{\theta} = 2\pi f_n+Z(\theta)F(2\pi f_c t), \quad (12)$$

where θ is the phase of the limit cycle, and $Z(\theta)$ is the phase response curve, which describes the sensitivity of the limit cycle oscillator against a slight perturbation at each phase. Besides, f_n and f_c are the natural and forcing frequency of the walker and the wobbling mass, respectively.

Define the phase difference Φ and frequency difference f_Δ between the limit cycle walker and the wobbling mass as:

$$\Phi := \theta-2\pi f_c t, \qquad f_\Delta := f_n-f_c. \quad (13)$$

Consequently, the dynamics of phase difference becomes:

$$\dot{\Phi} = 2\pi f_\Delta+\Gamma(\Phi), \quad (14)$$

where, $\Gamma(\Phi)$ is an averaged function that describes the phase coupling:

$$\begin{aligned}\Gamma(\Phi) &= \langle Z(\Theta+\Phi)F(\Theta)\rangle\\ &= \frac{1}{2\pi}\int_0^{2\pi} Z(\Theta+\Phi)F(\Theta)\mathrm{d}\Theta, \quad (15)\end{aligned}$$

and $\Theta := 2\pi f_c t$. Entrainment phenomenon occurs when the condition $\dot{\Phi} = 0$ is satisfied. In other words, the phase difference Φ becomes constant.

B. Entrainment Speed Maximization

The basic formulas for minimizing the average transient time required to entrain a phase model in the neighborhood of it have been introduced in [21]. Here we apply the formulas to our indirectly controlled limit cycle walker.

Define the steady phase difference in the entrained limit cycle as Φ^*, according to Eq. (14), the following condition should be satisfied to converge to it:

$$2\pi f_\Delta + \Gamma(\Phi^*) = 0. \tag{16}$$

To maximize the entrainment speed when Φ nears Φ^*, the convergence speed of $\Gamma(\Phi)$ with respect to Φ, *i.e.*, $|\Gamma'(\Phi)|$, should be maximized. In addition, by taking time derivative on both sides of Eq. (14), following equation is obtained:

$$\ddot{\Phi} = \dot{\Phi}\Gamma'(\Phi). \tag{17}$$

Notice that the signs of $\ddot{\Phi}$ and $\dot{\Phi}$ should be opposite to guarantee $\dot{\Phi} \to 0$. Consequently, $\Gamma'(\Phi)$ must be negative. Therefore the task is to maximize the following equation:

$$\arg\max_{F(\Theta)} = -\Gamma'(\Phi^*), \tag{18}$$

with the constraints of averaged power of the waveform:

$$\langle F(\Theta)^2 \rangle = E, \tag{19}$$

and Eq. (16). By rearranging the Eqs. (16-19), the following cost function is obtained:

$$\begin{aligned} \Sigma[F(\Theta)] \;=\; & -\Gamma'(\Phi^*) \\ & +\sigma(\langle F(\Theta)^2 \rangle - E) \\ & +\varepsilon(\Gamma(\Phi^*) + 2\pi f_\Delta), \end{aligned} \tag{20}$$

where σ and ε are Lagrange multipliers. By substituting Eq. (15) and its derivative with respect to Φ into Eq. (20), we got:

$$\begin{aligned} \Sigma[F(\Theta)] \;=\; & -\langle Z'(\Theta+\Phi^*)F(\Theta)\rangle \\ & +\sigma(\langle F(\Theta)^2\rangle - E) \\ & +\varepsilon(\langle Z(\Theta+\Phi^*)F(\Theta)\rangle + 2\pi f_\Delta) \\ =\; & \frac{1}{2\pi}\int_0^{2\pi} (F(\Theta)(-Z'(\Theta+\Phi^*) + \\ & \sigma F(\Theta) + \varepsilon Z(\Theta+\Phi^*)) \\ & -\sigma E + 2\pi f_\Delta \varepsilon) \mathrm{d}\Theta. \end{aligned} \tag{21}$$

Using the calculus of variations to find the optimal forcing waveform $F(\Theta)$, which maximizes the cost function, the following condition should be satisfied:

$$(-Z'(\Theta+\Phi^*) + 2\sigma F(\Theta) + \varepsilon Z(\Theta+\Phi^*)) = 0. \tag{22}$$

Therefore the optimal fast entrainment waveform, F_*, is derived accordingly:

$$F_*(\Theta) = \frac{1}{2\sigma}(Z'(\Theta+\Phi^*) - \varepsilon Z(\Theta+\Phi^*)). \tag{23}$$

This waveform, therefore, can be considered as a trade-off between $Z(\Theta+\Phi^*)$, which corresponds to the entrainment, and $Z'(\Theta+\Phi^*)$, which corresponds to the convergence speed. Next step is to determine the Lagrange multipliers σ and ε. By substituting Eq. (23) into Eq. (19) and Eq. (16), the following equations are obtained:

$$\frac{1}{4\sigma^2}(\langle (Z')^2\rangle - 2\varepsilon\langle Z'Z\rangle + \varepsilon^2\langle Z\rangle) = E, \tag{24}$$

$$\frac{1}{2\sigma}(\langle Z'Z\rangle - \varepsilon\langle Z^2\rangle) = -2\pi f_\Delta. \tag{25}$$

Since the period of Z is 2π, $\langle Z'Z\rangle$ vanishes by applying Fourier expansion on Z and Z'. Accordingly, ε is obtained as follows:

$$\varepsilon = \frac{4\pi f_\Delta \sigma}{\langle Z^2\rangle}. \tag{26}$$

Consequently, by substituting Eq. (26) into Eq. (23), F_* becomes:

$$F_*(\Theta) = \frac{Z'(\Theta)}{2\sigma} - \frac{2\pi f_\Delta Z(\Theta)}{\langle Z^2\rangle}, \tag{27}$$

where the Φ^* can be ignored since the process is asymptotic. Moreover, σ can be derived by substituting Eq. (26) into Eq. (24).

$$\sigma = -\frac{1}{2}\sqrt{\frac{\langle (Z')^2\rangle}{E - \frac{(2\pi f_\Delta)^2}{\langle Z^2\rangle}}}. \tag{28}$$

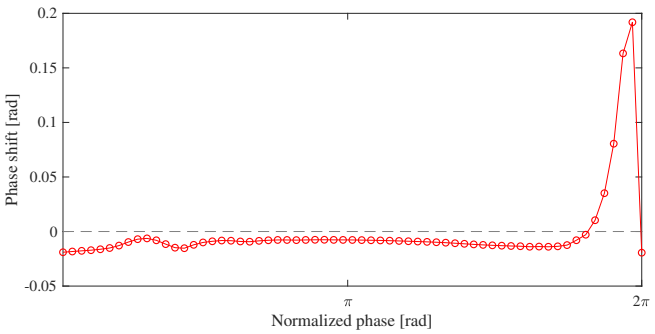

Fig. 2: Phase response curve

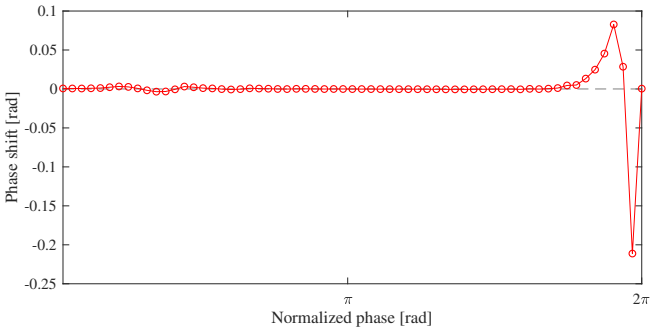

Fig. 3: Derivative of phase response curve with respect to phase

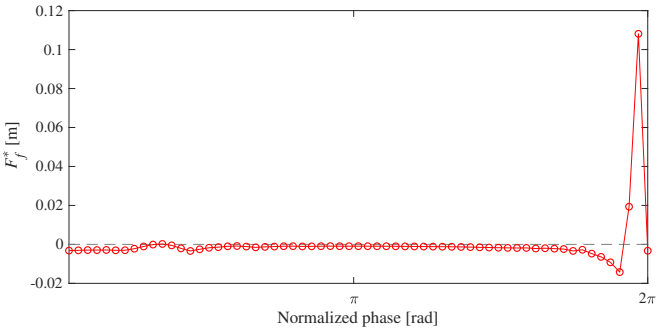

Fig. 4: Optimal fast entrainment waveform for $f_c = 1.62$ [Hz]

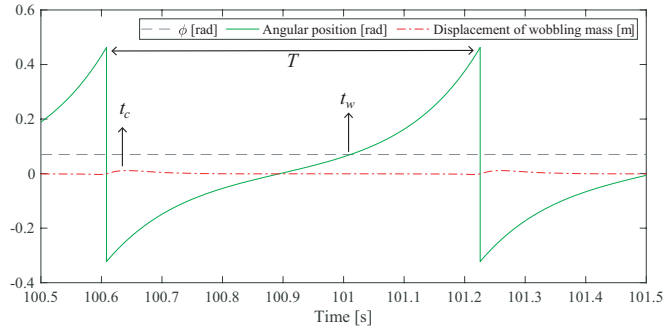

Fig. 5: Normalized phase difference between walker and wobbling mass in entrained limit cycle

From Eq. (27), we can understand that the shape of F_* is related to the frequency difference f_Δ, the phase response curve $Z(\Theta)$ and the derivative of it. The phase response curve $Z(\Theta)$ of this walker is numerically obtained by applying a slight perturbation at each phase of one whole steady walking cycle except the landing instant, which is similar to our previous study [22]. As shown in Fig. 2, the phase is normalized to $[0, 2\pi]$, where 0 corresponds to the instant immediately after landing, and 2π corresponds to the instant immediately before next landing. The limit cycle walker is, therefore, sensitive to the perturbations soon before feet landing. Since periodic oscillation of the wobbling mass is not applied yet, Φ is equivalent to Θ, by taking derivative of Z with respect to Θ, Z' is obtained as shown in Fig. 3.

Here we show an example of the optimal fast entrainment waveform F_* in one wobbling cycle by setting the forcing frequency to f_c=1.62 [Hz]. To normalize the waveform into a function with zero average, we further let: $F_*(\Theta) = F_*(\Theta) - \langle F_* \rangle$, and the obtained waveform is shown in Fig. 4.

IV. PERFORMANCE EVALUATION

In this section, we conduct numerical simulations to evaluate the performance of the optimal fast entrainment waveform we derived.

A. Phase Recovery

To compare their speed of phase recovery, we use the normalized phase difference of steady entrained gait for evaluation. In the entrained limit cycle walking, the steady phase difference between the walker and wobbling mass is defined as follows:

$$\psi := \frac{2\pi(t_c - t_w)}{T}. \tag{29}$$

As shown in Fig. 5, t_c [s] is the instant at which the wobbling mass reaches its local maximum and t_w [s] is the instant at which the stand-feet are perpendicular to the ground ($\theta_1 = \phi$). In addition, T [s] is the step period. Then, we slightly disturb the entrained limit cycle at different phases of a whole cycle, and count the steps required for returning to the original steady phase. One should notice that theoretically, the required steps should be infinite horizon [23]. However, we numerically judge the convergence when the deviation

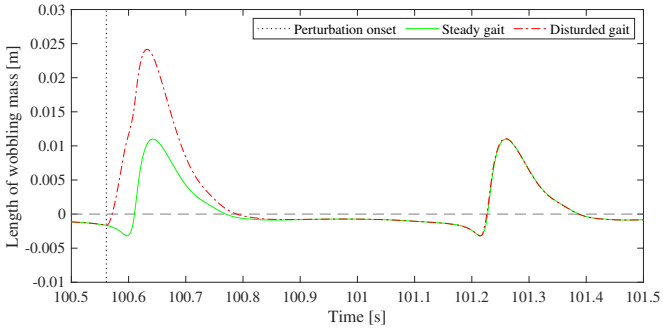

(a) Applying perturbation

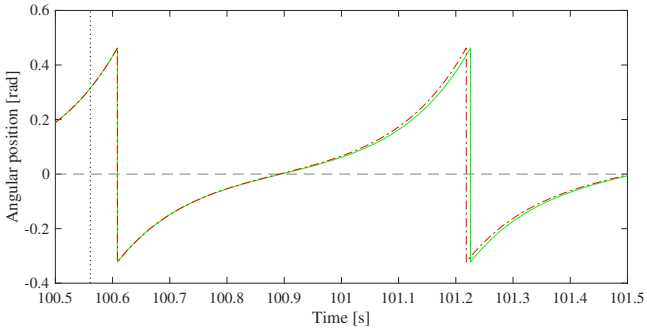

(b) Phase shift induced by perturbation

Fig. 6: Perturbation and phase shift

between the phase difference of the current step and steady gait is less than 10^{-3}. Consequently, the following process is conducted:

(A1) Start locomotion with Eq. (3) and (7) until converge to steady gait using the parameters listed in Tab. I.
(A2) Calculate the phase difference in steady gait and save the instant t_s [s] and state $\boldsymbol{q}(s)$, $\dot{\boldsymbol{q}}(s)$ immediately after the ground collision of the last step.
(A3) Start locomotion from t_s and use $\boldsymbol{q}(s)$, $\dot{\boldsymbol{q}}(s)$ as initial conditions. In addition, change the desired forcing waveform from F to $F + 0.05$ [m] within the duration $[d_0 \quad d_f]$ [s]. The sudden change in the desired forcing waveform, which is shown in Fig. 6 (a), leads to a slight perturbation to the system as shown in Fig. 6 (b). Here the perturbation onset d_0 [s] is initialized as t_s and

$$d_f = d_0 + d_\Delta, \tag{30}$$

where $d_\Delta = 0.03$ [s] is the perturbation duration.
(A4) save ψ for 60 steps.
(A5) Increase d_0 by d_Δ [s].
(A6) Repeat from (A3) to (A5) until the perturbation onset $d_0 = t_s + T$.

An example of returning to the entrained limit cycle of F_* after perturbation is shown in Fig. 7.

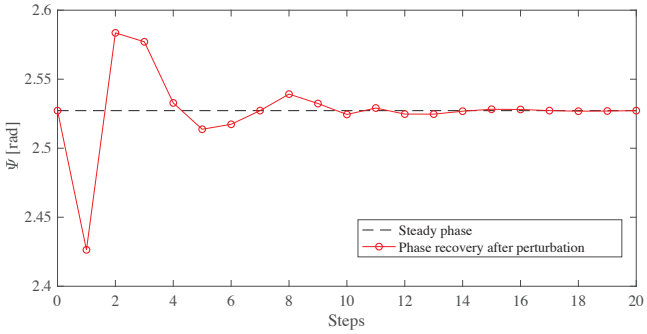

Fig. 7: Phase recovery after perturbation

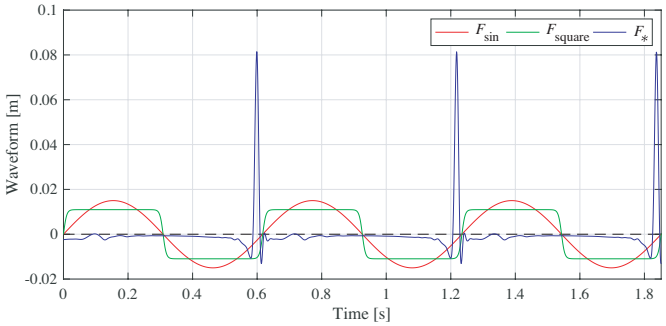

Fig. 8: Candidate waveform for comparison

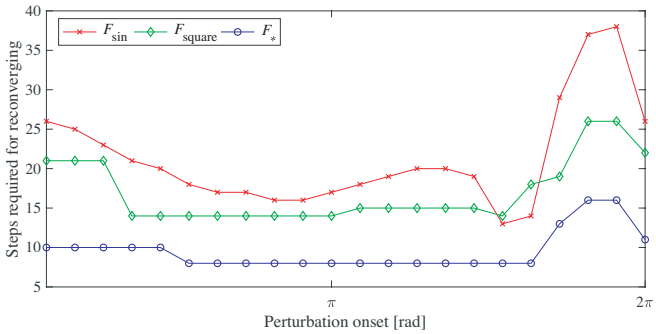

(a) Steps required for phase recovery

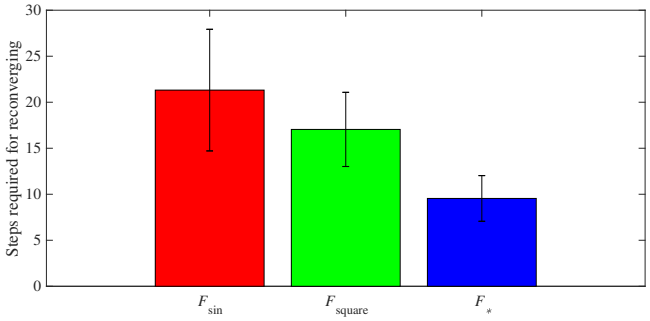

(b) Mean value and standard deviation of steps

Fig. 9: Comparison of steps required for recovery, where $f_c = 1.62$ [Hz]

B. Comparison with Other Examples

Next, we compare the optimal fast entrainment waveform with other typical examples, *i.e.*, sine waveform $F_{\sin}$ and square waveform F_{square}, which are commonly used as candidates for entrainment performance comparison in nonlinear dynamics. The waveform are defined as follows:

$$F_{\sin} = A_m \sin(2\pi f_c t), \tag{31}$$

$$F_{\text{square}} = \tilde{A}_m \tanh\left(c(\sin(2\pi f_c t))\right), \tag{32}$$

where A_m and $\tilde{A}_m$ denote the amplitude of them respectively, and c is a positive constant which adjusts the sharpness of tanh. To make a fair comparison, a convenient practical way is set to: $\langle F_{\sin}^2 \rangle = \langle F_{\text{square}}^2 \rangle = \langle F_*^2 \rangle$. Consequently, the power of waveform are normalized to equal by adjusting the amplitude, as shown is Fig. 8.

We first compare their performance with $f_c = 1.62$ [Hz], and the steps required for phase recovery with respect to the perturbation onset are shown in Fig. 9 (a). The results indicate that the optimal fast entrainment waveform F_* we derived achieves the best performance in all cases. In addition, we can see that the phase that requires the most steps for recovery of all these three waveform are soon before 2π, it is because the walker is sensitive when disturbing it soon before collision timings, which is consistent with the phase response curve. The averaged steps and standard deviation are shown in Fig. 9 (b). Statistically significant difference ($p < 0.001$) is detected for all the three groups. Moreover, according to post hoc comparisons using Fishers least significant difference, pairs of groups, whose means differ significantly ($p < 0.001$), are detected.

TABLE I: Parameter Settings

$m_1 (= m_2)$	1.0	kg
m_3	1.0	kg
m_c	0.01	kg
$L_1 (= L_2)$	0.15	m
L_3	0.20	m
ϕ	0.07	rad
g	9.81	m/s^2
A_m	0.02	m
c	10	

C. Evaluation with Respect to Frequency

To observe the overall performance, we compare the steps required for recovery with respect to forcing frequency. We should notice that the optimal fast entrainment waveform F_* exists only when $E > \frac{(2\pi f_\Delta)^2}{\langle Z^2 \rangle}$, according to Eq. (28), *i.e.*, the existence of F_* is constrained by the frequency difference f_Δ between the forcing frequency and the walker's natural frequency, since the desired forcing power E and the phase response curve Z are already determined. Consequently, the theoretical boundary for this example is $f_c \in [1.54 \quad 1.64]$. The walker can be entrained by the optimal fast entrainment waveform F_* within this whole range. In contrast, the sine waveform $F_{\sin}$ and square waveform F_{square} can entrain the

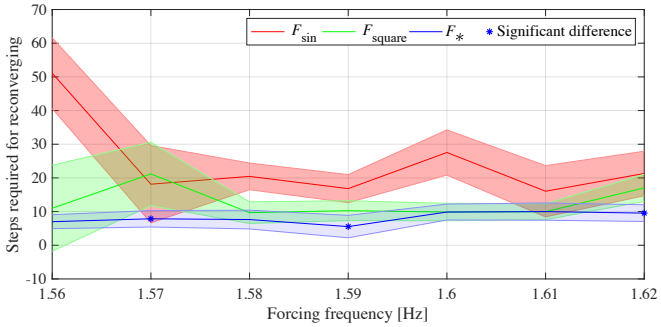

Fig. 10: Comparison of steps required for recovery versus to forcing frequency

walker only within $f_c \in [1.56 \quad 1.62]$. Within this range, we calculate the mean value and standard deviation of the required steps for recovery, which is shown in Fig. 10. The averaged required steps of F_* is less than $F_{\sin}$ in all conditions. Besides, it is also less than F_{square} in most cases except $f_c = 1.60$ and 1.61 [Hz]. Statistically significant difference ($p < 0.01$) is detected at $f_c = 1.57, 1.58, 1.59$ and 1.62 [Hz]. However, test on post hoc comparisons reports that the difference between F_* and F_{square} is not significant when $f_c = 1.58$ [Hz].

V. CONCLUSION AND FUTURE WORK

In this paper, we mathematically derived an optimal fast entrainment waveform for the indirectly controlled limit cycle walker against external perturbations based on the phase reduction theory. Numerical simulation results show that the waveform we derived requires the least steps for recovery to entrained limit cycle among all candidates. However, it is difficult to guarantee a statistically significant difference in the whole range of forcing frequency. This issue can be ascribed to the fact that the dynamics of the theoretical phase model is continuous and smooth, while the dynamics of the walking robot is discontinuous, due to the state jumps induced by feet landing event. Therefore, an enhanced method may consider this limit cycle walker as a hybrid dynamical system which takes the feet landing into account [24], alternatively, the current method can be more appropriate for the locomotion robots with smooth dynamics, *e.g.*, sliding locomotion robots on slippery ground [25] [26], which inherently avoid ground collisions.

REFERENCES

[1] A. Goswami, B. Espiau and A. Keramane, "Limit cycle walking and their stability in a passive bipedal gait," *Proceedings of the IEEE International Conference on Robotics and Automation*, pp. 246-251, 1996.

[2] T. McGeer, "Passive dynamic walking," *International Journal of Robotics Research*, Vol. 9, No. 2, pp. 62-82, 1990.

[3] D. G. E. Hobbelen and M. Wisse, "A disturbance rejection measure for limit cycle walkers: The gait sensitivity norm," *IEEE Transactions on Robotics*, Vol. 23, No. 6, pp. 1213-1224, 2007.

[4] F. Iida and T. Russ, "Minimalistic control of biped walking in rough terrain," *Autonomous Robots* Vol. 28, No. 3, pp. 355-368, 2010.

[5] C. Maufroy, H. Kimura and T. Nishikawa, "Stable dynamic walking of the quadruped Kotetsu using phase modulations based on leg loading/unloading against lateral perturbations," *Proceedings of the IEEE International Conference on Robotics and Automation*, pp. 1883-1888, 2012.

[6] F. Asano and X. Xiao, "Role of deceleration effect in efficient and fast convergent gait generation," *Proceedings of the IEEE International Conference on Robotics and Automation*, pp. 5669-5674, 2013.

[7] F. Asano and I. Tokuda, "Indirectly controlled limit cycle walking of combined rimless wheel based on entrainment to active wobbling mass," *Multibody System Dynamics*, Vol. 34, Iss. 2, pp. 191-210, 2015.

[8] J. Ackerman and J. Seipel, "Energy efficiency of legged robot locomotion with elastically suspended loads," *IEEE Trans. on Robotics*, Vol. 29, Iss. 2, pp. 321-330, 2013.

[9] D. Li, T. Li, Q. Li, T. Liu and J. Yi, "A simple model for predicting walking energetics with elastically-suspended backpack," *Journal of Biomechanics*, Vol. 49, Iss. 16, pp. 4150-4153, 2016.

[10] I. S. Young, R. M. Alexander, A. J. Woakes, P. J. Butler and L. Anderson, "The synchronization of ventilation and locomotion in horses (Equus Caballus)," *The Journal of Experimental Biology*, Vol. 166, No. 1, pp. 19-31, 1992.

[11] L. C. Rome, L. Flynn and T. D. Yoo, "Biomechanics: Rubber bands reduce the cost of carrying loads," *Nature*, Vol. 444, No. 7122, pp. 1023-1024, 2006.

[12] L. Li, I. Tokuda and F. Asano. "Nonlinear analysis of an indirectly controlled limit cycle walker," *Artificial Life and Robotics*, Vol. 23, Iss. 4, pp. 508-514, 2018.

[13] L. Li, Fumihiko Asano, Isao Tokuda, "High-frequency vibration of leg masses for improving gait stability of compass walking on slippery downhill," *Journal of Robotics and Mechatronics*, Vol. 31, No. 4, pp. 621-628, 2019.

[14] H. Nakao, "Phase reduction approach to synchronisation of nonlinear oscillators," *Contemporary Physics*, Vol. 57, No. 2, pp. 188214, 2016.

[15] F. Asano, Y. Akutsu and I. Tokuda, "Gait control of combined rimless wheel using active wobbling mass that vibrates backward and forward," *Proceedings of the International Conference on Ubiquitous Robots and Ambient Intelligence*, pp. 340-345, 2013.

[16] Y. Hanazawa, T. Hayashi, M. Yamakita and F. Asano, "High-speed limit cycle walking for biped robots using active up-and-down motion control of wobbling mass," *Proceedings of the IEEE/RSJ International Conference on Intelligent Robots and Systems*, pp. 3649-3654, 2013.

[17] Y. Hanazawa, "Development of rimless wheel with controlled wobbling mass," *Proceedings of the IEEE/RSJ International Conference on Intelligent Robots and Systems*, pp. 4333-4339, 2018.

[18] Y. Kuramoto, "Chemical Oscillations, Waves, and Turbulence," *Springer*, Berlin, 1984.

[19] J. Guckenheimer, "Isochrons and Phaseless Sets," *Journal of Mathematical Biology*, Vol. 1, Iss. 3, pp. 259-273, 1975.

[20] P. Goel and B. Ermentrout, "Synchrony, stability, and firing patterns in pulse-coupled oscillators," *Physica D: Nonlinear Phenomena*, Vol. 163, No. 3-4, pp. 191-216, 2002.

[21] A. Zlotnik, Y. Chen, I. Z. Kiss, H. Tanaka and J. Li. "Optimal waveform for fast entrainment of weakly forced nonlinear oscillators," *Physical Review Letters* Vol. 111, Iss. 2, pp. 024102, 2013.

[22] L. Li, I. Tokuda and F. Asano, "Optimal input waveform for an indirectly controlled limit cycle walker," *Proceedings of the IEEE/RSJ International Conference on Intelligent Robots and Systems*, pp. 7454-7459, 2018.

[23] J. B. Rawlings and K. R. Muske. "The stability of constrained receding horizon control," *IEEE Transactions on Automatic Control*, Vol. 38, No. 10, pp. 1512-1516, 1993.

[24] S. Shirasake, W. Kurebayashi and H. Nakao, "Phase reduce theory for hybrid nonlinear oscillators," *Physical Review E*, Vol. 95, Iss. 1, pp. 012212, 2017.

[25] L. Li, F. Asano and I. Tokuda, "Nonlinear analysis of an indirectly controlled sliding locomotion robot," *Proceedings of the IEEE/RSJ International Conference on Intelligent Robots and Systems*, pp. 8221-8226, 2018.

[26] L. Li, F. Asano, I. Tokuda, "High-speed sliding locomotion generation on slippery surface of an indirectly controlled robot with viscoelastic body," *IEEE Robotics and Automation Letters*, Vol. 4, Issue 3, pp. 2950-2957, 2019.